Computational Simulations of Supramolecular Hydrogen-Bonded Aggregates: $HubM_3$, $FlexM_3$, and Adamantane-Based Hubs in Chloroform

Donovan N. Chin, Dana M. Gordon, and George M. Whitesides*

Contribution from the Department of Chemistry, Harvard University, Cambridge, Massachusetts 02138

Received June 20, 1994[⊗]

Abstract: The relative stabilities of four aggregates composed of 1 equiv of a tris-melamine and 3 equiv of neohexyl isocyanurate were investigated using molecular mechanics and dynamics; the results from the simulations were compared with experiments. The relative deviation from planarity (DP) of the cyanuric acid−melamine ($CA_3{\cdot}M_3$) rosette correlated with stability in this series of aggregates. The amount of distortion in the aggregate was computed using a Langevin dynamics simulation (using a structure inferred from ^1H NMR experiments) of a system comprising the aggregate and four molecules of chloroform. These four molecules of chloroform made particularly important contributions to the conformational behavior and stability of the aggregate, as judged by the results of a simulation of fully-solvated $HubM_3{\cdot}(RCA)_3$ (that is, one explicitly including solvent molecules). One molecule of chloroform seemed to occupy a unique position in the center of the aggregate and to contribute strongly to the stability of these aggregates. The order of stabilities suggested by the relative values of DP is $HubM_3{\cdot}(RCA)_3$ > AdM_3 II·$(RCA)_3$ > $FlexM_3{\cdot}(RCA)_3$ > AdM_3 I·$(RCA)_3$ (Schame 1). This order was confirmed by ^1H NMR competition experiments (AdM_3 I·$(RCA)_3$ was not observed as a stable complex). The rationale for the relationship between the DP and the stabilities of the aggregates, and the influence of solvation by chloroform on these stabilities, is discussed.

Introduction

Although hydrogen-bonded aggregates based on the cyanuric acid−melamine ($CA_3{\cdot}M_3$) rosette motif are proving to be an excellent system with which to study molecular self-assembly and noncovalent synthesis,[1−3] the design of new aggregates, and the prediction of their stabilities, remains a substantially empirical activity. The purpose of the work described in this paper was to define the value of molecular mechanics[4] and dynamics[5] in correlating the structures of the molecules constituting these aggregates with their experimental stabilities. Accomplishing this objective required defining the proper protocols for using computational methods, since, as a group, these aggregates pose a number of problems. First, comparisons of absolute energies computed for complexes of distinct composition and structure are not straightforward, and it is necessary to find a measure of relative stabilities that does not require absolute energies. Second, the correct treatment of solvent remains an issue.[6] Although these studies were carried out in chloroform—a relatively simple solvent—the influence of solvent on the results is profound (as we will demonstrate). Establishing an economical and cost-effective protocol for treating solvent computationally requires making and validating approximations. Third, a valid approach to estimating the contributions of entropies of formation to the stabilities of the complexes must be established.[7] Methods for using molecular dynamics to estimate entropies are still being developed, and none has proved clearly satisfactory for complex molecules.[8,9] Fourth, the problem of sampling conformational space must be solved in a way that identifies minima in conformational energies that are global rather than local. Fifth, since these computations are intended to go hand-in-hand with an experimental program, and to be useful to physical−organic chemists, they must be implemented in a protocol that is reasonably efficient in terms of its requirements for computational time.

This study focused on aggregates of a single class: that comprising tris-melamines ($HubM_3$ and congeners thereof) and neohexyl isocyanurate (RCA) (Scheme 1). We have tested the ability of computational methods to predict and rationalize trends in stabilities observed in these aggregates on changing the structure of the tris-melamines. An important inference from this work is that the amplitudes of vibration for the M and CA groups out of the plane of the $CA_3{\cdot}M_3$ rosette correlate with the stabilities of the aggregates. This metric allows comparisons of different structures in different solvents and is reasonably efficient in computational time; it is, of course, a *relative* method, and although it is intuitively reasonable, its justification ultimately rests on correlation of experiment, computation and physical intuition.

Specifically, we focused on the examination of four aggregates: $HubM_3{\cdot}(RCA)_3$, $FlexM_3{\cdot}(RCA)_3$, AdM_3 I·$(RCA)_3$, and AdM_3 II·$(RCA)_3$ (Scheme 1). Syntheses of $HubM_3$, $FlexM_3$, and RCA have been reported previously.[2] Schemes 2 and 3 outline the syntheses of AdM_3 I and AdM_3 II, respectively.

Model and Methodology

Adaptation of Modeled Aggregates. All calculations were done using the CHARMm 22 force field.[10,11] We constructed

[⊗] Abstract published in *Advance ACS Abstracts,* December 1, 1994.

(1) Seto, C. T.; Whitesides, G. M. *J. Am. Chem. Soc.* **1991**, *113*, 712.
(2) Seto, C. T.; Whitesides, G. M. *J. Am. Chem. Soc.* **1993**, *115*, 905.
(3) Seto, C. T.; Whitesides, G. M. *J. Am. Chem. Soc.* **1993**, *115*, 1321.
(4) Clark, T. *A Handbook of Computational Chemistry*; Wiley: New York, 1987.
(5) For a review, see: McCammon, J. A.; Harvey, S. C. *Dynamics of proteins and nucleic acids*; Cambridge University Press: Cambridge, 1987.
(6) See ref 5, pp 41−44.
(7) Smith, D. E.; Zhang, L.; Haymet, D. J. *J. Am. Chem. Soc.* **1992**, *114*, 5875.
(8) Edholm, O.; Berendsen, H. J. C. *Mol. Phys.* **1984**, *51*, 1011.
(9) Karplus, M.; Kushick, J. N. *Macromolecules* **1981**, *14*, 325.
(10) Brooks, B. R.; Bruccoleri, R. E.; Olafson, B. D.; States, D. J.; Swaminathan, S.; Karplus, M. *J. Comput. Chem.* **1983**, *4*, 187.

0002-7863/94/1516-12033$04.50/0

Scheme 1. Supramolecular Complexes Considered[a]

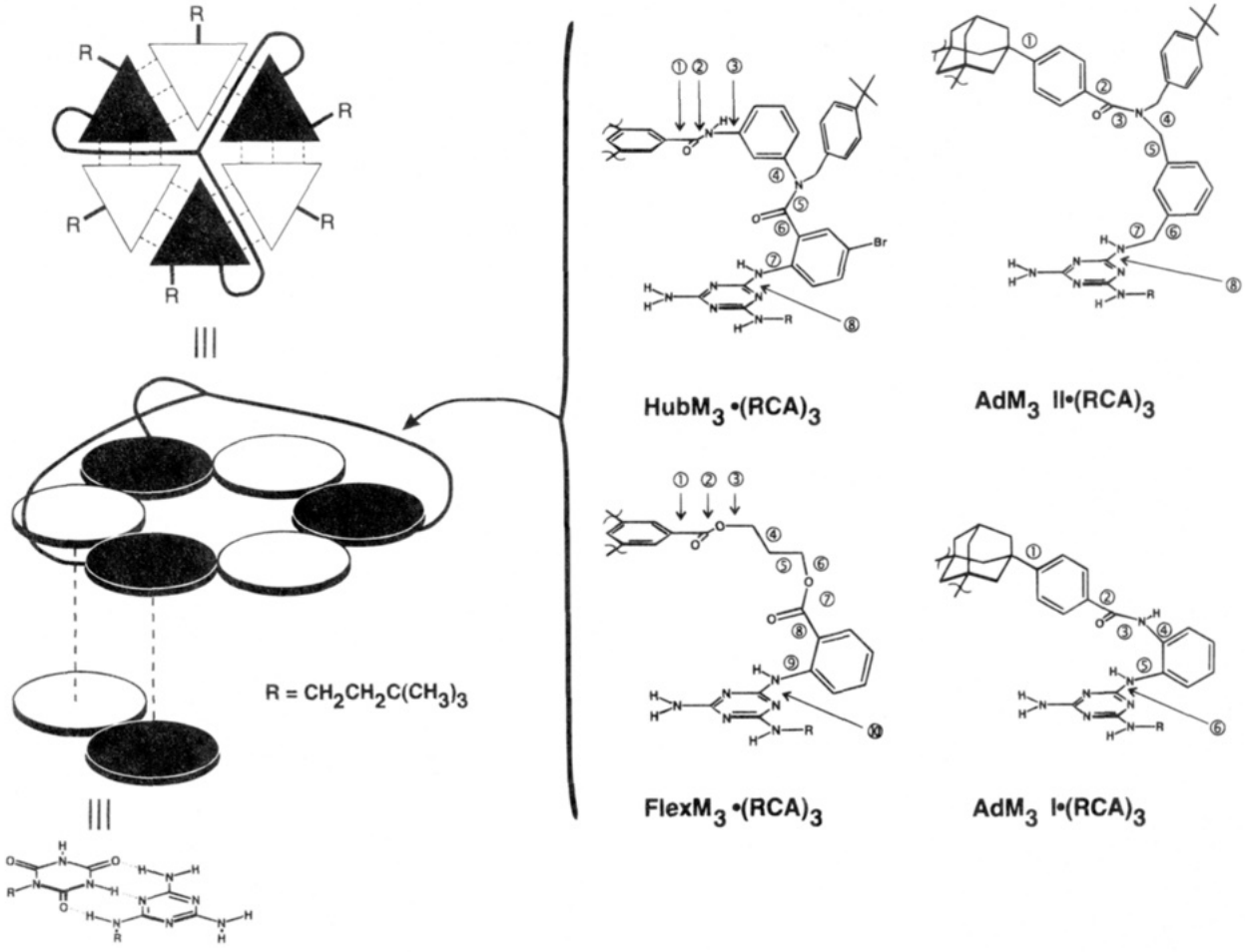

[a] The circled numbers on the spokes represent labels for the families of torsional angles. Each family contains the three structurally symmetric torsional angles of the tris-melamine spokes.

Scheme 2. Synthesis of AdM_3 I[a]

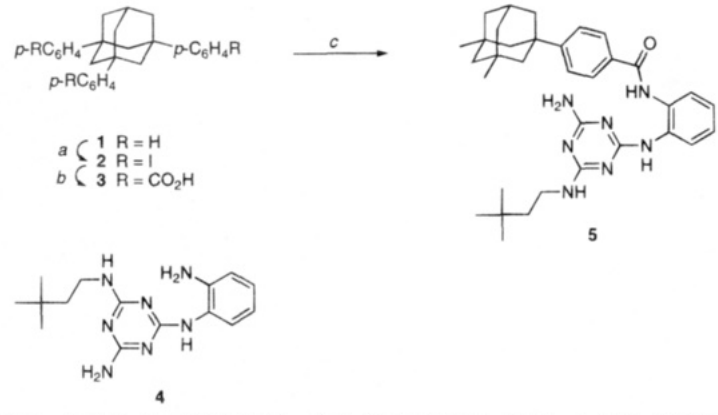

[a] Key: (a) I_2, $PhI(O_2CCF_3)_2$, $CHCl_3$, rt, 94%; (b) *t*-BuLi, THF, −78 to 0 °C; CO_2 (g), 0 °C to rt, 79%; (c) $(COCl)_2$, DMF, THF, rt; **4**, $(i\text{-Pr})_2NEt$, THF, 0 °C to rt, 69%.

the neo-hexyl isocyanurates and tris-melamines using standard valence geometries with the QUANTA 3.3 molecular modeling program.[12] An extended atom representation was used for all nonpolar alkyl groups.[10] The melamine and isocyanurate groups of the complexes were initially set to a planar geometry with a distance of 1.8 Å assigned to hydrogen bonds.[13] The complexes were assembled around the $CA_3{\cdot}M_3$ rosette (Scheme 1), and the torsional angles in the spokes of the tris-melamines (excluding −CONH− torsional angles) were rotated so that the center of the tris-melamine was at its maximum distance from the plane of the $CA_3{\cdot}M_3$ rosette. The torsional angles were also rotated to maintain the average C_3 symmetry of the complexes inferred from NMR experiments.[2] Energetically unfavorable steric interactions in the complexes were relaxed by performing 1000 steps of the conjugate gradient energy-minimizing algo-

(11) *QUANTA 3.3 Parameter Handbook*, MSI: Burlington, MA, 1992. Frey, R. F.; Coffin, J.; Newton, S. Q.; Ramek, M.; Cheng, V. K. W.; Momany, F. A.; Schäfer, L. *J. Am. Chem. Soc.* **1992**, *114*, 5369. Schäfer, L.; Newton, S. Q.; Momany, F. A.; Klimkowski, J. V. *J. Am. Chem. Soc.* **1992**, *114*, 5369.

(12) QUANTA 3.3 molecular modeling program, MSI, 1992.

(13) Pranata, J.; Wierschke, S. G.; Jorgensen, W. L. *J. Am. Chem. Soc.* **1991**, *113*, 2810.

Scheme 3. Synthesis of AdM_3 II

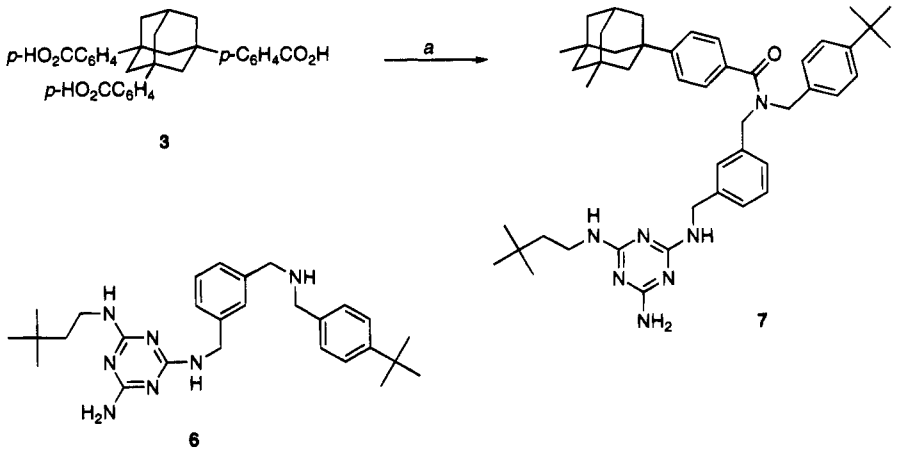

[a] Key: (a) $(COCl)_2$, DMF, THF, rt; **6**, $(i\text{-Pr})_2NEt$, THF, 0 °C to rt, 50%.

rithm;[10] the resulting configurations served as the starting points for further structural refinements.

To facilitate these analyses, the three structurally symmetrical torsional angles of the spokes of the tris-melamine were grouped into "families." As an example, $HubM_3$ was categorized into the following torsional families (labeled 1–8 in Scheme 1): 1, three secondary benzamide carbon–carbon bonds; 2, three secondary benzamide amide bonds; 3, three secondary anilide carbon–nitrogen bonds; 4, three tertiary anilide carbon–nitrogen bonds; 5, three tertiary benzamide amide bonds; 6, three tertiary benzamide carbon–carbon bonds; 7, three bromobenzamide carbon–nitrogen single bonds; and 8, three triazine carbon–nitrogen single bonds.

Simulations in Vacuum. An initial simulation in vacuum was carried out for $HubM_3$·$(RCA)_3$. The nonbonded interactions were cut off beyond 15 Å, and a switching function[10] was used to smooth electrostatic and van der Waals energies to 0 between 11 and 14 Å. A distance-dependent dielectric constant was used in this simulation.

The energy of $HubM_3$·$(RCA)_3$ was minimized to an energy gradient of 0.06 kcal/mol·Å using adopted basis Newton Raphson[10] (ABNR) as a precursor for a molecular dynamics simulation (MD). A MD calculation was carried out by integrating Newton's equation of motion with the Verlet[14] algorithm using a time step of 1 fs; SHAKE[15] was used to constrain the high-frequency motions of covalent bonds to hydrogen atoms and, thus, allow for numerical stability in the integration with a 1 fs time step. The system was "heated," by assigning velocities from a Gaussian distribution in 5 K increments, from 0 to 300 K, over a 4 ps stage. The heating stage was followed by an equilibration stage of 5 ps, during which the system was checked periodically to see if the temperature was within ±5 K of the targeted temperature (300 K). If the temperature was outside the desired range, the velocities were rescaled to give the targeted temperature. The final phase of the simulation was carried out for 10 ps without rescaling the velocities.

Simulations in Solution: Explicit Solvation of $HubM_3$·$(RCA)_3$ with Constant Pressure and Temperature (CPT) Molecular Dynamics. Fully-solvated $HubM_3$·$(RCA)_3$ was analyzed to study its behavior and interactions with chloroform. This complex was placed in the center of a cubic box with dimensions of 26 Å on a side. A modified Monte Carlo algorithm[12] (Boltzmann temperature set at 300 K) placed 84 molecules of chloroform in the cubic box around the complex under periodic boundary conditions.[16] To maintain the structure of the aggregate, it was necessary to place a single molecule of chloroform in the center of the complex (we will discuss this requirement, and the consequences if it was not followed, when comparing the results of simulations of $HubM_3$·$(RCA)_3$, both in vacuum and in solution).

The energy of the entire solvated complex was then minimized with *unconstrained* box dimensions according to the following prescription: (a) the complex was fixed in Cartesian space, and the solvent–solvent and solvent–complex interactions were allowed to relax using 100 steps of steepest descents;[10] (b) constraints on the Cartesian coordinates were removed, and the energy of the entire system was minimized with 1000 steps of ABNR. The nonbonded conditions were the same as those used in the simulations in vacuum.

The Berendsen constant pressure and temperature (CPT) MD algorithm[17] was used to carry out an 80 ps simulation at 1 atm and 300 K. Covalent bonds to hydrogen were constrained utilizing the SHAKE method,[15] and a simulation time step of 1 fs was used. The temperature and pressure coupling values were set at 0.4 and 5.0 ps, respectively,[18] and the isothermal compressibility was set at 5.0×10^{-5} atm. The nonbonded conditions were the same as those in the simulation in vacuum except that a dielectric constant of 1.0 was used.

Simulations in Solution: Implicit Solvation of $HubM_3$·$(RCA)_3$ with Langevin Dynamics. To reduce the amount of computational effort required with solvated complexes, a Langevin dynamics algorithm[19–21] was used that explicitly included only a small number of molecules of solvent and that represented the remaining excluded molecules of solvent by a *potential of mean force* term. The Langevin dynamics algorithm is defined by eq 1,[22] where **r** is the atomic position vector of

$$m_i\ddot{\mathbf{r}}_i = \mathbf{F}_i(t) - \gamma_i m_i \dot{\mathbf{r}}_i(t) + \mathbf{A}_i(t) \qquad (1)$$

(14) Verlet, L. *Phys. Rev.* **1967**, *153*, 250.
(15) van Gunsteren, W. F.; Berendsen, H. J. C. *Mol. Phys.* **1977**, *34*, 1311.
(16) Allen, M. P.; Tildesley, D. J. *Computer Simulations of Liquids*; Oxford University Press: Oxford, 1987.
(17) Berendsen, H. J. C.; Postma, J. P. M.; van Gunsteren, W. F.; DiNola, A.; Haak, J. R. *J. Chem. Phys.* **1984**, *81*, 3684.
(18) The value of 0.4 is based on experience, 5.0 is from the CHARMm online documentation.
(19) Levy, R. M.; Karplus, M.; McCammon, J. A. *Chem. Phys. Lett.* **1979**, *65*, 4.
(20) Widman, G.; Pastor, R. W. *J. Chem. Soc., Faraday Trans.* **1992**, *88*, 1747.
(21) . Brunger, A.; Brooks, C. L.; Karplus, M. *Chem. Phys. Lett.* **1984**, *105*, 495.
(22) Chandrasekhar, S. *Rev. Mod. Phys.* **1943**, *15*, 1.

atom i, m is the atomic mass, and $\mathbf{F}_i(t)$ is the systematic force[10] on atom i arising from interactions with other atoms at time t. The term $\mathbf{A}_i(t)$ is a randomly fluctuating force that is assumed to be uncorrelated with the atomic positions and velocities and is Gaussian with zero mean and variance given by eq 2, where

$$\langle \mathbf{A}_i(t)\mathbf{A}_i(t')\rangle = 2m_i\gamma_i kT\delta(t-t') \tag{2}$$

k is the Boltzmann constant, T is the temperature, $\delta(t-t')$ is the Dirac δ function, and γ_i is the collisional frequency. The dissipating term, $-\gamma_i m_i \dot{\mathbf{r}}_i(t)$, is a velocity-dependent force that implies that the medium absorbs energy as the atom moves through it; the collisional frequency, γ, characterizes the rate at which this energy is exchanged.

The collisional frequency can be determined from the mass-normalized Stokes relationship assuming stick boundary conditions for the frictional coefficient (eq 3);[23] in this equation, i is

$$\gamma_i = \frac{\zeta_i}{m_i} = 6\pi\eta\sigma_i \tag{3}$$

the index labeling the atom, ζ is the frictional coefficient, η is the viscosity of chloroform at 298 K (η = 0.542 cP),[24] m_i is the atomic mass (kg) of atom i, and σ_i is the *effective* atomic radius (Å) calculated from the accessible surface area[25] of atom i (using the Lee and Richards algorithm[26] with a probe of zero radius). The calculated average value of 38 ps^{-1} for γ was used in all subsequent simulations involving the Langevin equation.

We used $HubM_3$·$(RCA)_3$ as a test case with which to compare the Langevin model (with a system comprising four molecules of chloroform and aggregate) and a fully-solvated model (84 molecules of chloroform and aggregate). The nonbonded conditions were the same as those in the simulation in vacuum except that a distance-dependent dielectric term was used.[10] This term approximated the mean-field Coulombic force caused by atoms that were ignored in the reduced-particle Langevin simulation. The average structure of the complex and the four molecules of chloroform with the lowest energies of interaction (see Figure 2 and the section describing results from CPT calculations), averaged over the last 20 ps of the 80 ps CPT simulation of the fully-solvated system, were used as a starting point for the Langevin simulation. The energy of $HubM_3$·$(RCA)_3$·$4CHCl_3$ was first minimized by the conjugate gradient method (100 steps), followed by minimization to a gradient less than 1.0×10^{-8} kcal/mol·Å using ABNR. The collisional frequencies were assigned, and a 60 ps Langevin dynamics simulation at 300 K was then carried out on $HubM_3$·$(RCA)_3$·$4CHCl_3$ and the results were compared to the fully-solvated CPT model. In the simulation, SHAKE was applied to covalent bonds to hydrogens, and a time step of 1 fs was used. Langevin simulations on the remaining complex·$4CHCl_3$ systems, following the procedure used for $HubM_3$·$(RCA)_3$·$4CHCl_3$, were carried out for 60 ps.

Comparisons of Torsional Fluctuations. Autocorrelation functions[27,28] (ACFs) for fluctuations of torsional angles about their mean values were computed for various torsional families

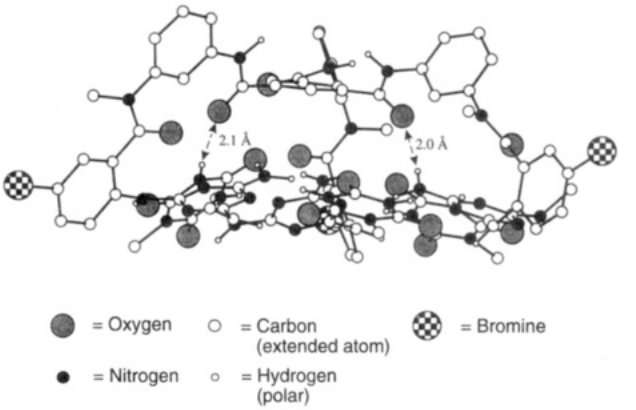

Figure 1. Ball and stick representation of $HubM_3$·$(RCA)_3$ after 7 ps of MD in vacuum. Some atoms are deleted for clarity. Severe distortions are beginning to occur as the melamine groups are pulled toward the amide bonds adjacent to the aromatic hub. Several of these amide bonds have deviated from planarity with the central aromatic group due to strong electrostatic interactions with the melamines and isocyanurate groups.

of $HubM_3$·$(RCA)_3$ from the Langevin simulation (using four molecules of chloroform) and the CPT simulation (84 molecules of chloroform). The normalized autocorrelation function, $C(t)$, is defined by eq 4:

$$C(t) = \frac{\langle \Delta\phi(t)\Delta\phi(0)\rangle}{\langle \Delta\phi(0)^2\rangle} \tag{4}$$

The property $\Delta\phi_n(t)$ is the fluctuation of a torsional angle about its time averaged position, $\Delta\phi_n(t) = \phi_n(t) - \langle\phi_n\rangle$, where the brackets, $\langle ...\rangle$, denote the average of the nth torsion, ϕ_n, over the time of the analysis.

Comparisons of the Root-Mean-Square Atomic Fluctuations. The magnitudes of the atomic displacements observed in the CPT and Langevin simulations were computed by calculating the root-mean-square (RMS) atomic fluctuations,[29] $\langle \Delta\mathbf{u}_i^2\rangle^{1/2}$, of the simulated structures as defined by eq 5, where

$$\langle \Delta\mathbf{u}_i^2\rangle^{1/2} = \sqrt{\frac{\sum_{n=1}^{N}(\mathbf{r}_i - \langle\mathbf{r}_i\rangle)^2}{N}} \tag{5}$$

$\mathbf{r}$ is the atomic coordinate of the atom i, and $\langle\mathbf{r}_i\rangle$ is its average over the number of frames,[30] N, in the trajectory.

Results and Analysis

Molecular dynamics simulations of $HubM_3$·$(RCA)_3$ were carried out in vacuum and in a fully-solvated environment (CPT dynamics). In order to construct a model of a solvated complex that might be used in the economical Langevin dynamics method, we determined the influence of solvent in this system. After parameterization of the Langevin system, all of the aggregates were analyzed.

Simulation of $HubM_3$·$(RCA)_3$ *in Vacuo*. Efforts to simulate $HubM_3$·$(RCA)_3$ *in vacuo* were unsuccessful. Strong electrostatic attractions between the atoms of the CA_3·M_3 rosette and the amide groups adjacent to the benzene ring in the center of the tris-melamine caused catastrophic distortions in the complex during the first 7–9 ps of the heating and equilibration phase of the MD simulation (Figure 1). The same distortions were

(23) Jost, W. *Diffusion in Solids, Liquids, and Gasses*; Academic Press: New York, 1960.
(24) *CRC Handbook of Chemistry and Physics*; Weast, R. C., Ed.; CRC Press: Boca Raton, 1984.
(25) Pastor, R. W.; Karplus, M. *J. Phys. Chem.* **1988**, *92*, 2636.
(26) Lee, B.; Richards, F. M. *J. Mol. Biol.* **1971**, *55*, 379.
(27) Zwanzig, R. *Annu. Rev. Phys. Chem.* **1965**, *16*, 67.
(28) Kushick, J. In *Statistical Mechanics*; Berne, B. J., Ed.; Modern Theoretical Chemistry; Plenum Press: New York, 1977; Vol. 6, Chapter 2.
(29) Elber, R.; Karplus, M. *Science* **1987**, *235*, 318.
(30) A "frame" corresponds to a set of atomic coordinates recorded every 0.5 ps.

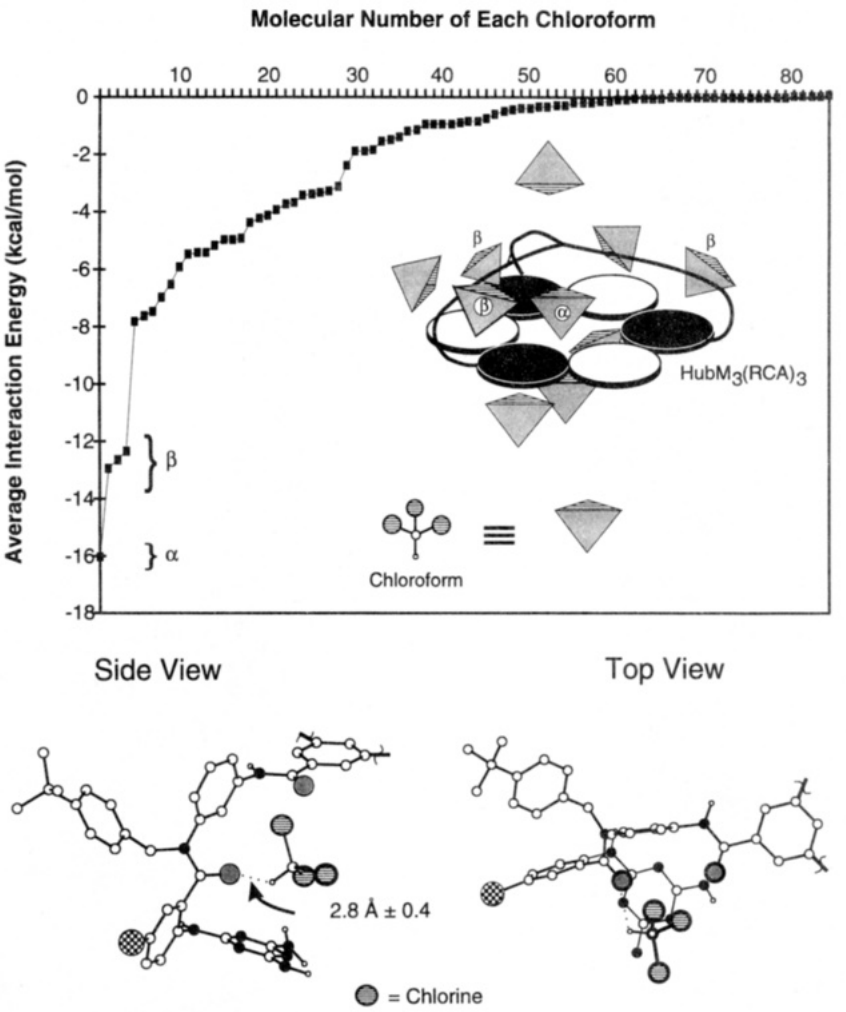

Figure 2. (Top) Average energy of interaction between molecules of chloroform and $HubM_3{\cdot}(RCA)_3$ taken from a 20 ps segment of CPT dynamics. The average chloroform−complex energies of interaction are sorted from strongest to weakest energy (left to right on the *x*-axis). The schematic shows the average positions (the averaged structure was briefly minimized to reduce any geometrical artifacts due to the averaging) for the 10 most strongly interacting (lowest energies) molecules of chloroform around the aggregate. (Bottom) Detailed view of the orientation of a β chloroform to a spoke of $HubM_3(RCA)_3$. This view was taken from a structure averaged over the last 20 ps of the simulation (the averaged structure was briefly minimized to eliminate any geometrical artifacts due to the averaging). Some atoms are omitted for clarity.

observed during attempts to minimize the initial conformation to an energy gradient less than 0.01 kcal/mol·Å. The distortions resulted in a structure that was inconsistent with the one suggested by ^{1}H NMR spectroscopy.[2] This result suggested that the role of molecules of solvent is important in maintaining the geometry inferred from ^{1}H NMR.

CPT Simulations of Solvated $HubM_3{\cdot}(RCA)_3$. The inward folding of $HubM_3{\cdot}(RCA)_3$ in the simulation in vacuum suggested that a single molecule of chloroform might occupy the center of the complex. NMR spectroscopy of these classes of aggregates suggested that, in some cases, aggregates that encapsulate a molecule of chloroform can be observed as separate entities, but that both solvent-free and solvent-containing species are stable in chloroform.[40] These spectra demonstrate that, in addition, the solvent-containing aggregate is more stable than the solvent-free aggregate. A single molecule of chloroform was easily accommodated at the center of the complex without distortion in the simulation. Corroborating evidence for the inclusion of a single chloroform molecule in the center of the aggregate (and the other aggregates investigated here) came from a simulation of an analog of AdM_3 I (a tris-melamine having a carboxylic acid group on the fourth vertex of the adamantyl group) complexed with three RCA molecules in the same fully-solvated chloroform environment. In a simulation in which this analog did not have a molecule of chloroform in the center of the complex at the beginning of the simulation, one molecule of chloroform diffused into the center of the complex (after 40 ps) and stayed there for the rest of the simulation (100 ps).

Conformation of $HubM_3{\cdot}(RCA)_3$. $HubM_3{\cdot}(RCA)_3{\cdot}84CHCl_3$ maintained the coplanarity of its $CA_3{\cdot}M_3$ rosette throughout the 80 ps simulation and exhibited none of the structural distortions observed in the simulation in vacuum. The 3-fold symmetry of the complex was also maintained throughout the simulation, in keeping with the NMR data.[2]

Behavior of Solvent in the CPT Simulation. The behavior of solvent around $HubM_3{\cdot}(RCA)_3$ in the CPT simulation, carried out in the presence of 84 molecules of solvent with periodic boundary conditions, was analyzed by plotting the average nonbonded energy of interaction between each of these molecules of chloroform (over the last 20 ps interval of the simulation) and the aggregate (Figure 2 top). The locations of the four molecules of chloroform that interacted most strongly with the complex are shown, schematically, in Figure 2 top. One molecule of chloroform was located in the center of the complex (α), while each of the other three molecules of chloroform (β) were located above a CA·M pair. The molecules of chloroform marked "β" formed weak hydrogen bonds with the carbonyl groups of the spoke (Figure 2 bottom). The α and β molecules of chloroform did not exchange with other

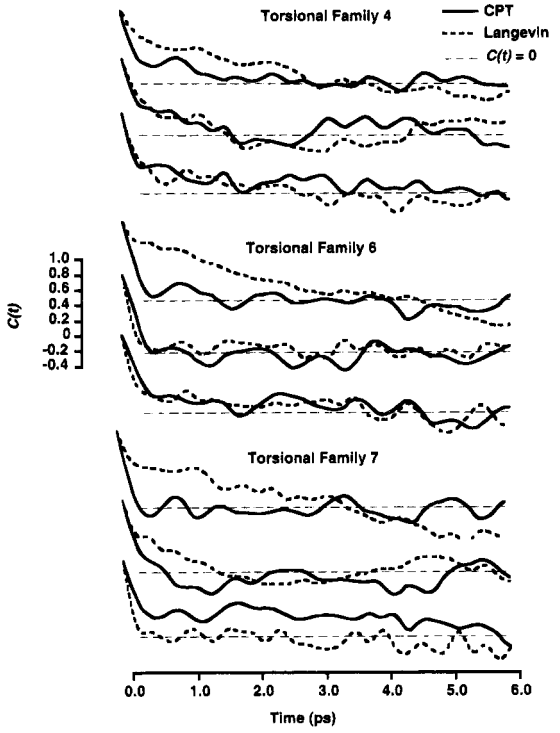

Figure 3. Profiles of the fluctuation in autocorrelation values of dihedral angles for torsional families. Data taken from 20 ps segments of CPT (solid lines) and Langevin dynamics (dashed lines) performed on $HubM_3$·$(RCA)_3$.

molecules of chloroform during the simulation. The average *calculated* diffusion coefficient[16] of the α and β types of chloroform was 6.17×10^{-7} cm²/s, while the average *simulated* diffusion coefficient of the bulk chloroform was 1.62×10^{-5} cm²/s (the simulated diffusion coefficient of bulk chloroform is in satisfactory agreement with the experimental value[31] of 3.3×10^{-5} cm²/s).

The results of the studies of solvation in the CPT simulation provided the basis for our decision to continue the simulations using only the four molecules of chloroform (α and β) that are most strongly associated with the aggregate, while representing the remaining molecules of solvent by an effective solvent potential (Langevin dynamics). The choice to represent only *four* molecules of solvent explicitly was arbitrary, to some extent. The four molecules of chloroform were chosen since the energy of interaction of this set was significantly larger than that of other molecules of solvent. The equilibrium geometry of $HubM_3$·$(RCA)_3$ in this approximation was very similar to that obtained using 84 molecules of chloroform.

Langevin Simulation of $HubM_3$·$(RCA)_3$: Comparison with the CPT Simulation. Torsional Relaxation. The ACFs of torsional fluctuations provide a portrait of the average decay of these fluctuations. If fluctuations are undamped in any way, they exhibit simple harmonic motion and thus the ACFs also exhibit harmonic behavior. In these systems, fluctuations resulted from complex interactions involving bonded and nonbonded forces; thus, the ACFs decayed with a profile that was characteristic of their environments.[32,33] The ACFs are, as a result, useful as a comparative measure of the environments for torsional fluctuations in $HubM_3$. Figure 3 shows values of $C(t)$ for selected torsional families of $HubM_3$. These plots show that, overall, the autocorrelation functions for the torsional families of $HubM_3$ have similar profiles in the CPT and Langevin simulations. Two torsional angles (the first profiles of families 6 and 7) appear not to have the damped behavior of their CPT counterparts; the quality of these profiles probably could be improved by using the collisional frequencies of *individual* atoms instead of the mean value for the collisional frequency of each type of atom. The time-dependent behavior of the torsional fluctuations of $HubM_3$, nevertheless, appeared to be modeled accurately by the method of Langevin dynamics with significant savings in computational time. The 60 ps Langevin simulation took approximately 2 h on an IBM 6000/550 workstation while the CPT simulation required 27 h.

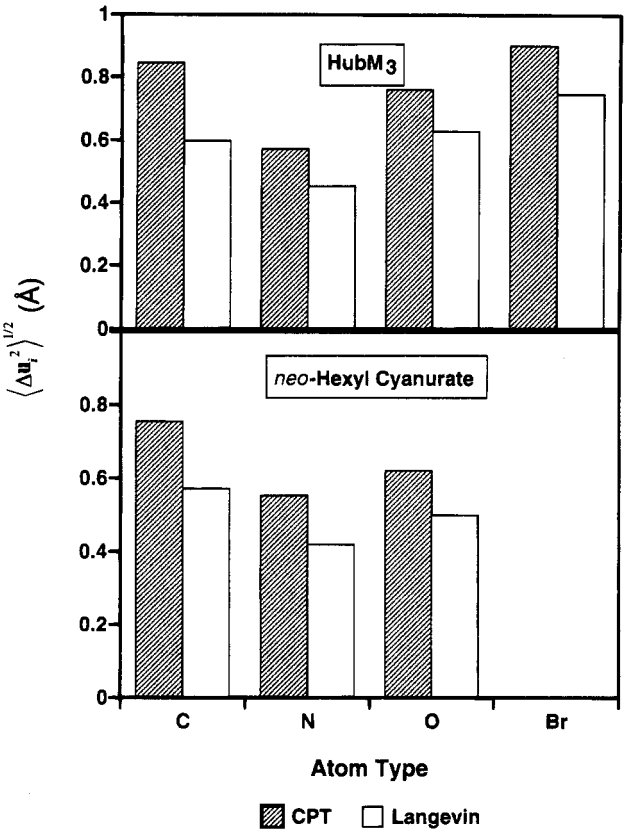

Figure 4. RMS atomic fluctuations averaged over types of atoms. These values were take from 20 ps CPT (filled bar) and Langevin dynamics (unfilled bar) simulations of $HubM_3$·$(RCA)_3$.

Magnitudes of Atomic Fluctuations. The values of $\langle \Delta \mathbf{u}_i^2 \rangle^{1/2}$ were averaged over the various types of atoms in $HubM_3$·$(RCA)_3$ from the last 20 ps of the Langevin and CPT dynamics (Figure 4). Figure 4 reflects similar magnitudes of atomic fluctuations in both the CPT and Langevin simulations. Values of $\langle \Delta \mathbf{u}_i^2 \rangle^{1/2}$ for similar atoms in similar locations in $HubM_3$·$(RCA)_3$ were comparable in the CPT and Langevin simulations.

On the basis of the similarity of the $\langle \Delta \mathbf{u}_i^2 \rangle^{1/2}$ and ACF data, we concluded that the reduced Langevin model compared favorably with the full CPT calculation for $HubM_3$·$(RCA)_3$. These simulations encouraged us to use the more economical Langevin simulations for investigations of other complexes.

Low Energy Complexes. Complexes of $FlexM_3$, AdM_3 I, and AdM_3 II with 3 equiv of RCA were modeled. These complexes were constructed following the prescription described for $HubM_3$·$(RCA)_3$ (C_3 symmetry, initially setting the melamines and cyanuric acid groups to a planar geometry with a hydrogen bond distance of 1.8 Å), with the four molecules of chloroform in the positions depicted in Figure 2. The energies of the solvated complexes were minimized initially with 100 steps of steepest descents and then "shaken" at 300 K for 10 ps using

(31) O'Reilly, D. E. *J. Chem. Phys.* **1968**, 5416.
(32) McCammon, J. A.; Wolnes, P. G.; Karplus, M. *Biochemistry* **1979**, *18*, 927.
(33) Brooks, C. L.; Brunger, A.; Karplus, M. *Biopolymers* **1985**, *24*, 843.

Langevin dynamics. The average structure for each complex, with the four associated molecules of chloroform, was computed based on the short sequence of Langevin dynamics. These averaged structures were each minimized further to an energy gradient of 1.0×10^{-8} kcal/mol·Å using ABNR, followed by 10 steps of Newton Raphson. The treatment of nonbonded interactions was the same as that used in the Langevin model of $HubM_3$·$(RCA)_3$.

Coplanarity in the Complexes. A central objective of this work was to develop a method of determining the relative stabilities of distinct complexes. It was not practical to estimate equilibrium constants (eq 6a), or free energies, since the

$$HubM_3 + 3\ RCA \overset{K}{\rightleftharpoons} HubM_3{\cdot}(RCA)_3 \qquad (6a)$$

$$HubM_3{\cdot}(RCA)_3 + AdM_3 \overset{K'}{\rightleftharpoons} HubM_3 + AdM_3{\cdot}(RCA)_3 \qquad (6b)$$

computational time required to form and dissociate the complex a statistically significant number of times in solution was prohibitive.[34] Simulations involving atomic scale force fields are, to date, only efficient in sampling events that occur on a subnanosecond time scale. Similar arguments also prohibited the determination of the equilibrium constant K' (eq 6b).

We have, therefore, searched for a surrogate for the stability of the complex that could be estimated easily by computation and applied efficiently to complexes with different structures and to complexes in different media. We have settled on the geometry of the CA_3·M_3 rosette, and in particular the planarity, or deviation from planarity, of the rosette (Figure 5). We hypothesized that (i) a stable complex would be associated with a planar CA_3·M_3 system and, conversely, that a less stable complex would be associated with a distortion from planarity and (ii) the extent of the distortion from planarity would correlate with the stability of the complex.

The deviation from planarity (DP) was easily measured in CHARMm by calculating the RMS deviation, in angstroms, between atoms in the CA_3·M_3 rosette and a plane fitted to these atoms by a least-squares method (Figure 5).[35] For computational convenience, the CA_3·M_3 rosette was defined as the non-hydrogen atoms in the melamine and isocyanurate groups of a complex. Figure 6 summarizes the calculated values of DP for the complexes under consideration. We predicted that the relative magnitudes of DP from the simulations would be inversely proportional to the relative experimental thermodynamic stabilities: That is, $HubM_3$·$(RCA)_3$ would be the most stable aggregate, followed by AdM_3 II·$(RCA)_3$ and then $FlexM_3$·$(RCA)_3$, and AdM_3 I·$(RCA)_3$ would be the least stable aggregate.

Langevin Dynamics. Conformational Analysis. Conformations accessible to the hubs around the structures of minimum energy were analyzed using a 60 ps Langevin simulation at 300

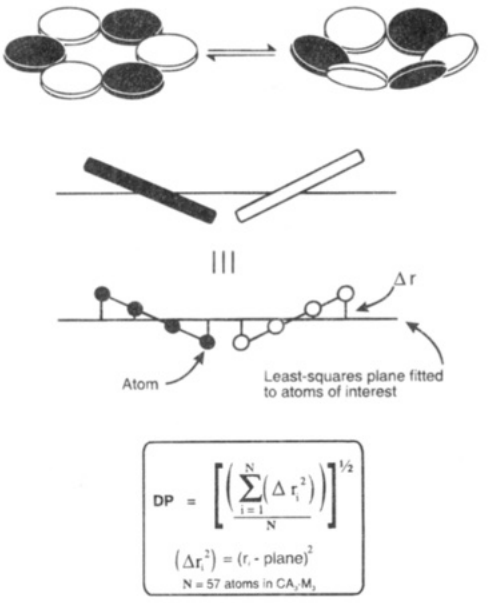

Figure 5. (Top) Relationship between a planar CA_3·M_3 system and distorted system. (Bottom) Schematic showing the calculation of DP.

K. The internal motions of interest were the torsional angles of the spokes of the tris-melamines. Torsional angles from conformations sampled every 0.2 ps were taken from the last 55 ps of the Langevin simulation (shown in Figure 7). Figure 7 is grouped along the *x*-axis into the torsional families of the hubs (Scheme 1). Each dash (−) corresponds to a torsional value (*y*-axis) in a particular conformation; corresponding torsional values of the minimized conformation are shown by "□" symbols. The order of the three sets of torsional values in each family is the same for each family: i.e., the first set of values in each family belong to one spoke, the second set of values belong to a second spoke, etc. Figure 7 underscores the range spanned by each torsional angle as well as the density of conformations having a torsional value within a particular range. The range of values for the torsional angles indicate that AdM_3 I is the most rigid member of this set. The torsional angles that comprise families 1 and 2 of AdM_3 I/II, while quite rotatable, are attached at the para position on the phenyl rings and, therefore, do not significantly influence the orientation of the spoke or the overall conformation of these adamantyl tris-melamines in the complexes. The average values of DP from the Langevin simulations are plotted in Figure 6; the average value of DP from the Langevin simulation for the AdM_3 I aggregate did not increase much from the value in the minimized state because its spokes were sufficiently rigid to prevent the CA_3·M_3 rosette from further distortion. These results show that the values of DP are influenced by the interplay between the torsional flexibility and the conformation of the spokes. We further rationalize the predicted order of relative thermodynamic stabilities in this way: (i) The spokes of $HubM_3$ preorganize the melamines in such a way that the value of DP is low, and the low conformational freedom in the spokes does not significantly distort the planar rosette. (ii) The spokes of AdM_3 II have a conformation that disrupts the planarity of the CA_3·M_3 rosette. These spokes are, however, more rigid than those of $FlexM_3$, and this rigidity results in an average value of DP that is lower than that for $FlexM_3$. (iii) $FlexM_3$ can form a planar CA_3·M_3 rosette but its flexible spokes allow the rosette to distort from coplanarity. (iv) AdM_3 I is more rigid than AdM_3 II but the conformation of its spokes disrupts the coplanarity of the rosette.

(34) It may be possible to use free energy perturbation methods that determine relative free energies ($\Delta\Delta G$) to explore the association of $HubM_3$ $FlexM_3$, or AdM_3 (I or II) with 3 equiv of RCA in solution. These methods would involve, for example, the "mutation" of $HubM_3$ into AdM_3 (I or II) in both the free and complexed states. While this method would yield results that were thermodynamically equivalent to measuring an equilibrium constant, and would be computationally less demanding than simulations involving a direct calculation of equilibrium constants, it would still be a prohibitively long simulation: mutation between the two structurally dissimilar hubs would require many steps in order to sample configurations adequately along the free energy path between the two final states in solution. See the following for further discussions: (a) Beveridge, D. L.; DiCapua, F. M. *Annu. Rev. Biophys. Biophys. Chem.* **1989**, *18*, 431. (b) van Gunsteren, W. F. *Protein Eng.* **1988**, *2*, 5. (c) Pranata, J.; Jorgensen, W. L. *Tetrahedron* **1991**, *14*, 2491. (d) Jorgensen, W. L. *J. Am. Chem. Soc.* **1989**, *111*, 3770. (e) Mitchell, M. J.; McCammon, A. J. *J. Comp. Chem.* **1991**, *12*, 271.

(35) Blow, D. M. *Acta Crystallogr.* **1960**, *13*, 168.

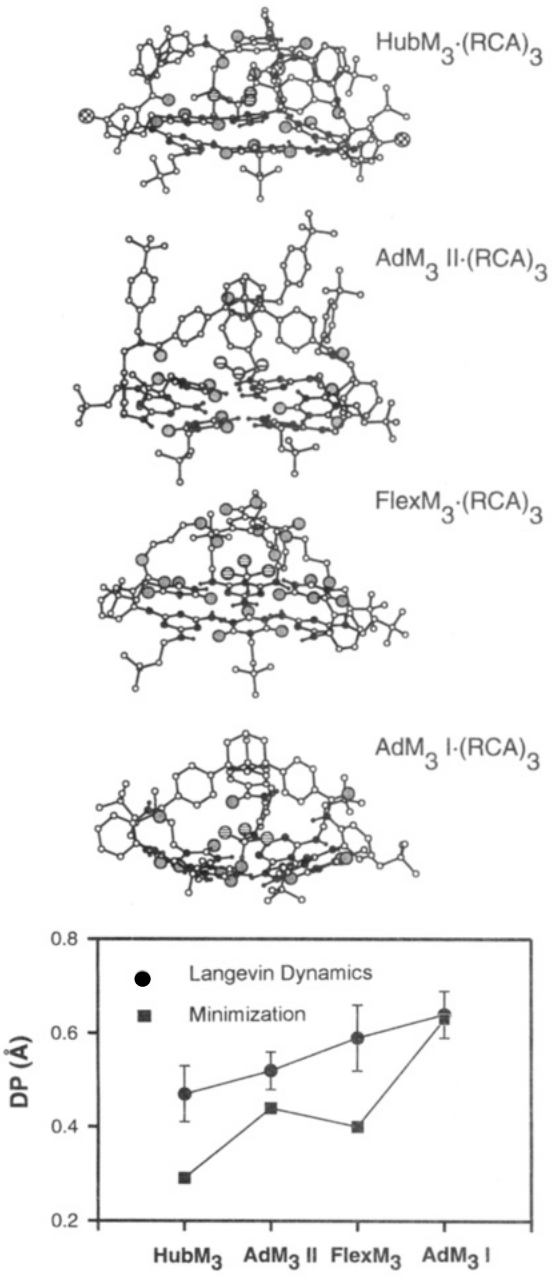

Figure 6. Values of DP calculated from the energy-minimized complexes (shown above plot) and from Langevin dynamics simulations (see text for a more complete description of these computations). For clarity, only the central chloroform molecule of the complex is shown.

Accessible Conformations during the Simulations. We wanted to gauge the number of different minima of the tris-melamines of the complexes that were sampled in the simulations, as well as the density of conformations around each minimum during the simulations. To study this distribution, the 55 ps Langevin simulation of the aggregates was sampled every 0.2 ps (275 structures). Each of these structures was minimized to an energy gradient of 0.001 kcal/mol·Å. The potential energy *of the tris-melamines* of each minimized aggregate was sorted into a histogram (Figure 8). This histogram shows the number of *different* conformations *of the tris-melamine* in the complex that was sampled during the 55 ps simulation; "different" conformations are defined as being separated by 2 kcal/mol. A characteristic feature of the distributions is that aggregates that were predicted to be more stable when compared with their counterparts ($HubM_3$ with $FlexM_3$; AdM_3 II with AdM_3 I) had more conformations that

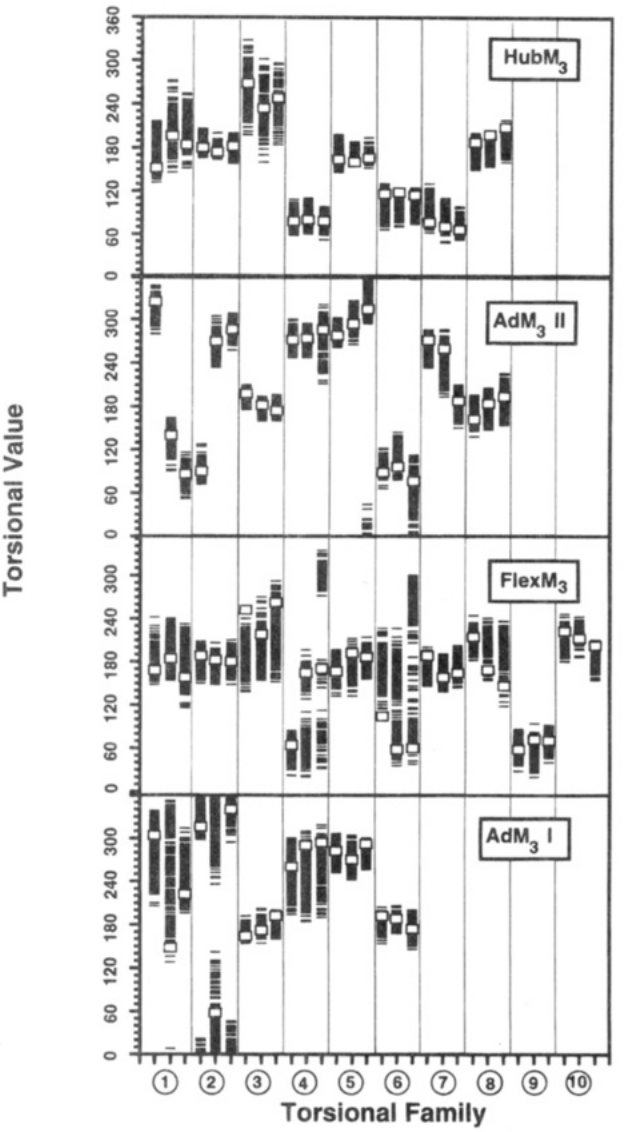

Figure 7. Values for each of the families of torsional angles (Scheme 1) from the 55 ps Langevin dynamics (−), sampled every 0.2 ps; torsional values of the energy-minimized structures (□) are also shown for reference.

were closer in energy over the length of the simulations. When the distributions were compared overall, aggregates that were more stable had distributions that were skewed toward their respective low energy minima. The distribution of substates for the adamantyl-based tris-melamines is compatible with the notion that the spokes of these molecules are relatively rigid; it is the out-of-plane orientation of the melamine groups by these spokes that limits the ability of these molecules to form complexes in chloroform that are as stable as the complex derived from $HubM_3$.

Competition Experiments in $CDCl_3$. To correlate the *predicted* hierarchies of stabilities of the various aggregates derived from computations with experiment, we carried out competition experiments of the type indicated by eq 6b. Uncomplexed tris-melamines ($HubM_3$, $FlexM_3$, or AdM_3 II) were added to solutions of preformed 1 + 3 aggregates ($HubM_3$·$(RCA)_3$, $FlexM_3$·$(RCA)_3$, or AdM_3 II·$(RCA)_3$) in $CDCl_3$, and the systems were examined by ^1H NMR spectroscopy. The region of the ^1H NMR spectra between δ 13 and 16 contains the NH protons of RCA in these aggregates; these signals are clearly separated from the rest of spectra and indicate the number and identity of complexes present in solution.[36] This region of

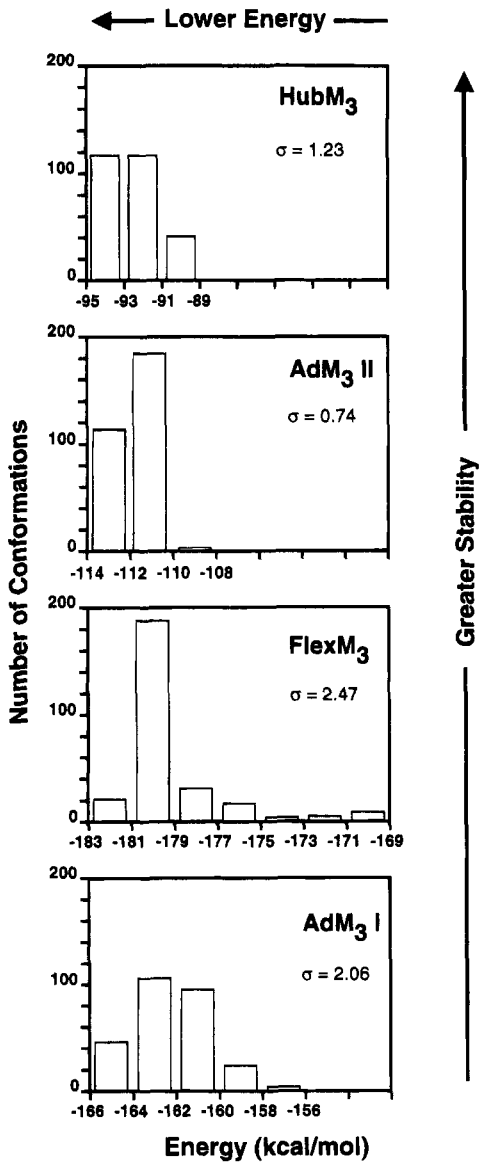

Figure 8. The distribution of minimized structures (0.001 kcal/mol·Å^2) from a 55 ps segment of the 60 ps Langevin simulation (σ is the standard deviation). Each bin is separated by 2 kcal/mol. Only bins that contain at least one conformation have values of energies associated with them. The plots are sorted in the order of most stable aggregate ($HubM_3$·$(RCA)_3$) to least stable aggregate (AdM_3 I·$(RCA)_3$).

the ^{1}H NMR spectra of each of the three homogeneous aggregates in $CDCl_3$ is distinct (see Figure 9(A, $HubM_3$·$(RCA)_3$; E, AdM_3 II·$(RCA)_3$; F, $FlexM_3$·$(RCA)_3$)); it was, therefore, possible to determine qualitatively the amount of each individual aggregate in mixtures of aggregates.

The first tris-melamine based on adamantane, AdM_3 I, was not observed to form a stable complex and not used in these competition experiments. Addition of RCA (3 equiv) to a solution of AdM_3 I in $CDCl_3$ gave a heterogeneous mixture; AdM_3 I did not appear to solubilize any of the added isocyanurate. There was no change in the ^{1}H NMR spectra of solutions of AdM_3 I in $CDCl_3$ after addition of RCA. On the basis of these observations, we concluded that AdM_3 I does not form a stable aggregate with RCA in $CDCl_3$.

The region of the ^{1}H NMR spectrum of $HubM_3$·$(RCA)_3$ (Figure 9A) in $CDCl_3$ between δ 13 and 16 contains *two* singlets assigned to the two types of isocyanurate NH protons present in a C_3-symmetric aggregate. This region of the spectrum of $FlexM_3$·$(RCA)_3$ (Figure 9F) in $CDCl_3$ contains *four* singlets. On the basis of the *relative* heights of the four peaks, we divide them into two sets of two singlets. Furthermore, we infer that each of these sets arises from a C_3-symmetric aggregate that is distinct on the NMR time scale. Another result of the flexibility of the spokes of $FlexM_3$ may, therefore, be its ability to adopt more than one stable, C_3-symmetric conformation in an aggregate with RCA in $CDCl_3$.

The low field region of the ^{1}H NMR spectrum of AdM_3 II·$(RCA)_3$ (Figure 9E) contains *one* very broad singlet. The spectrum of this aggregate remained virtually constant over a wide temperature range (223−313 K). Gel permeation chromatography (GPC) and vapor pressure osmometry indicated that these samples contain a *single* aggregate with a molecular weight within 20% of the theoretical weight of AdM_3 II·$(RCA)_3$, respectively (data not shown). Since the spokes of this tris-melamine are relatively rigid, and the shape of the GPC trace of this aggregate indicated stability roughly equal to that of $FlexM_3$·$(RCA)_3$,[37] we attribute the lack of resolution in these NMR spectra to conformational isomerization about the three adamantane−phenyl and three phenyl−carboxamide single bonds of AdM_3 II.

Addition of AdM_3 II (1 equiv) to a solution of $HubM_3$·$(RCA)_3$ resulted in a spectrum that was the superposition of the spectra of AdM_3 II and $HubM_3$·$(RCA)_3$ (Figure 9B). Conversely, addition of $HubM_3$ (1 equiv) to a solution of AdM_3 II·$(RCA)_3$ gave a spectrum indistinguishable from the spectrum derived from AdM_3 II and $HubM_3$·$(RCA)_3$ (Figure 9C). These results established that $HubM_3$·$(RCA)_3$ is more stable than AdM_3 II·$(RCA)_3$ in $CDCl_3$. The computational hierarchies of the stabilities of these aggregates based on values of DP from Langevin dynamics and minimizations successfully predicted the relative stabilities of these two aggregates (see Figure 6).

Addition of AdM_3 II (1 equiv) to a solution of $FlexM_3$·$(RCA)_3$ in $CDCl_3$ resulted in a spectrum that was the superposition of the spectra of AdM_3 II·$(RCA)_3$ and $FlexM_3$ (Figure 9G). Conversely, addition of $FlexM_3$ (1 equiv) to a solution of AdM_3 II·$(RCA)_3$ gave a spectrum (Figure 9H) indistinguishable from the spectrum derived from AdM_3 II and $FlexM_3$·$(RCA)_3$. These results established that AdM_3 II·$(RCA)_3$ is more stable than $FlexM_3$·$(RCA)_3$ in $CDCl_3$. Interestingly, AdM_3 II·$(RCA)_3$, the aggregate with the less well resolved ^{1}H NMR spectrum (Figure 9J) in $CDCl_3$, appears to be more thermodynamically stable, based on GPC peak shape and these results, than $FlexM_3$·$(RCA)_3$ whose ^{1}H NMR spectrum (Figure 9F) is well resolved. The predictions of the relative stability of these aggregates differ depending on whether the values of DP considered are those derived from minimizations or Langevin dynamics. The values of DP for these two aggregates derived from minimizations predict $FlexM_3$·$(RCA)_3$ will be more stable than AdM_3 II·$(RCA)_3$, whereas the values of DP derived from Langevin dynamics predict the opposite relative stabilities for these aggregates. The fact that the results from the dynamic simulation more closely approximate the experimental results in this system underscores the desirability of making predictions based on a dynamic rather than a static model. In cases in which the difference in the thermodynamic stability between two states is "small," subtle effects may be neglected in a static model.

Addition of $FlexM_3$ (1 equiv) to a solution of $HubM_3$·$(RCA)_3$ in $CDCl_3$ resulted in a spectrum that was the superposition of

(36) Simanek, E. E.; Wazeer, M. I. M.; Mathais, J. P.; Whitesides, G. M. *J. Org. Chem.* **1994**, *59*, 4904.

(37) Whitesides, G. M.; Simanek, E. E.; Mathais, J. P.; Seto, C. T.; Chin, D. N.; Mammen, M.; Gordon, D. M. *Acc. Chem. Res.*, in press.

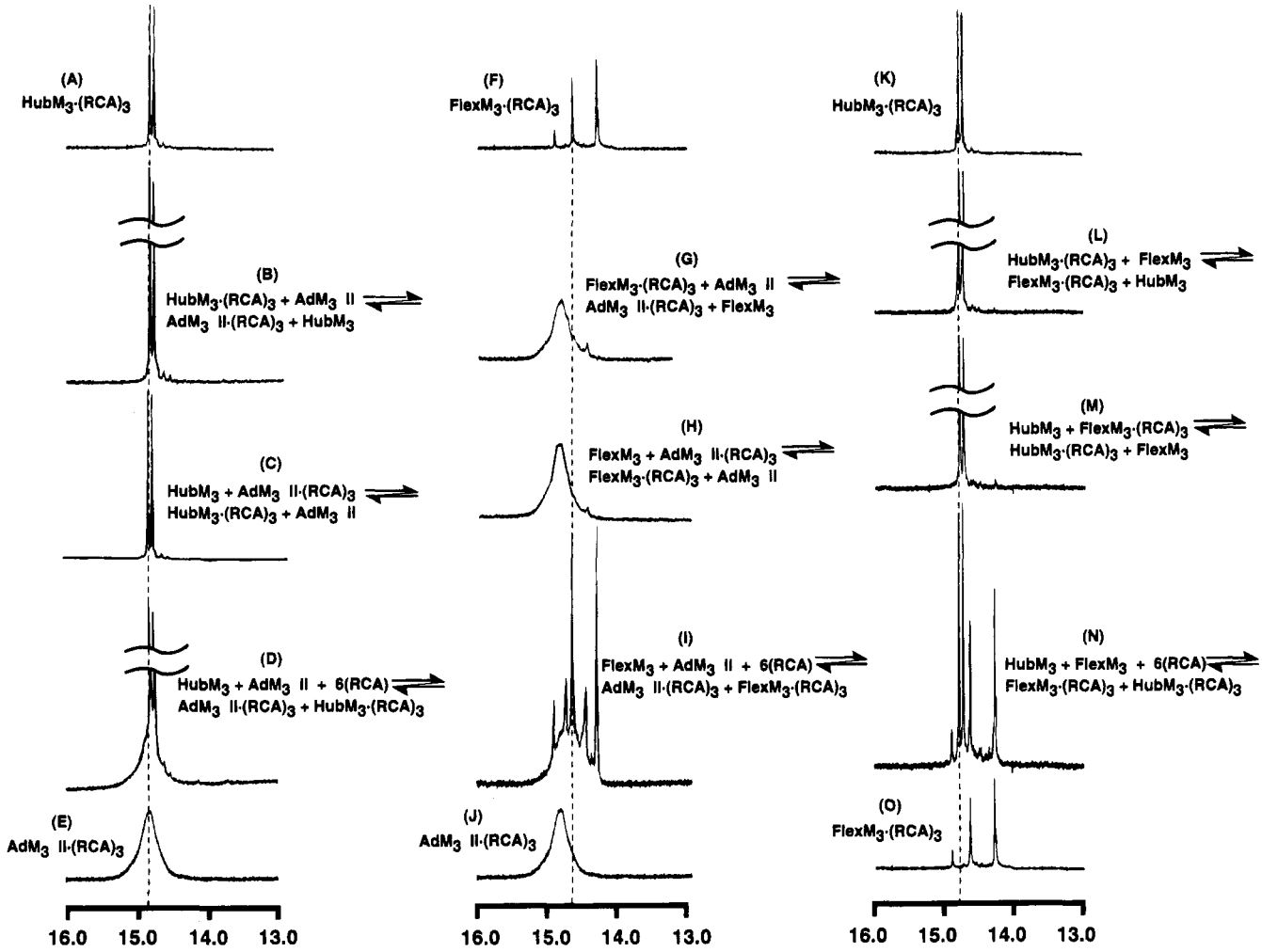

Figure 9. Portions of ^{1}H NMR spectra (500 MHz): (A) $HubM_3$·$(RCA)_3$ (5 mM in $CDCl_3$). Mixtures at equilibrium resulting from addition of a second tris-melamine (1 equiv) to a solution of a preformed 1 + 3 aggregate (5 mM in $CDCl_3$): (B) $HubM_3$·$(RCA)_3$ + AdM_3 II; (C) $HubM_3$ + AdM_3 II·$(RCA)_3$. (D) Mixture at equilibrium derived from $HubM_3$, AdM_3 II (5 mM in $CDCl_3$), and RCA (6 equiv). (E) AdM_3 II·$(RCA)_3$ (5 mM in $CDCl_3$). Portions of ^{1}H NMR spectra (500 MHz): (F) $FlexM_3$·$(RCA)_3$ (5 mM in $CDCl_3$). Mixtures at equilibrium resulting from addition of a second tris-melamine (1 equiv) to a solution of a preformed 1 + 3 aggregate (5 mM in $CDCl_3$): (G) $FlexM_3$·$(RCA)_3$ + AdM_3 II; (H) $FlexM_3$ + AdM_3 II·$(RCA)_3$. (I) Mixture at equilibrium derived from $FlexM_3$, AdM_3 II, (5 mM in $CDCl_3$) and RCA (6 equiv). (J) AdM_3 II·$(RCA)_3$ (5 mM in $CDCl_3$). Portions of ^{1}H NMR spectra (500 MHz): (K) $HubM_3$·$(RCA)_3$ (5 mM in $CDCl_3$). Mixtures at equilibrium resulting from addition of a second tris-melamine (1 equiv) to a solution of a preformed 1 + 3 aggregate (5 mM in $CDCl_3$): (L) $HubM_3$·$(RCA)_3$ + $FlexM_3$; (M) $HubM_3$ + $FlexM_3$·$(RCA)_3$. (N) Mixture at equilibrium derived from $HubM_3$, $FlexM_3$, (5 mM in $CDCl_3$) and RCA (6 equiv). (O) $FlexM_3$·$(RCA)_3$ (5 mM in $CDCl_3$).

the spectra of $FlexM_3$ and $HubM_3$·$(RCA)_3$ (Figure 9L). Addition of $HubM_3$ (1 equiv) to a solution of $FlexM_3$·$(RCA)_3$ gave a spectrum (Figure 9M) indistinguishable from the spectrum derived from $FlexM_3$ and $HubM_3$·$(RCA)_3$. This set of experiments confirmed the computational prediction that $HubM_3$·$(RCA)_3$ is more stable than $FlexM_3$·$(RCA)_3$ in $CDCl_3$.

Addition of RCA (3 equiv) to the equilibrium mixtures derived from $HubM_3$, AdM_3 II, and RCA (3 equiv) gave spectra that were the superposition of the spectra of the two individual 1 + 3 aggregates (Figure 9D). These results implied that $HubM_3$·$(RCA)_3$ and AdM_3 II·$(RCA)_3$ did not interact strongly in $CDCl_3$. Analogously, addition of RCA (3 equiv) to the equilibrium mixtures containing $HubM_3$, $FlexM_3$, and RCA (3 equiv) resulted in spectra containing only lines attributable to the two 1 + 3 aggregates (Figure 9N); $HubM_3$·$(RCA)_3$ and $FlexM_3$·$(RCA)_3$ did not appear, therefore, to interact discernibly in $CDCl_3$. In contrast to these two systems, addition of RCA (3 equiv) to the equilibrium mixtures containing AdM_3 II, $FlexM_3$, and RCA (3 equiv) did not result in spectra that were the simple superposition of the spectra of the two homogeneous 1 + 3 aggregates (Figure 9I). These spectra contain the lines that appear in the spectra of the individual aggregates and two additional lines for which we are presently unable to account. The presence of these resonances was *not* a function of the concentration of the sample, the presence or absence of excess RCA in the sample, or the procedure followed in preparation of the sample. These observations suggested that these resonances were *not* due to associations between the aggregates, the presence of excess RCA in solution, or the existence of metastable equilibria in this system, respectively. At present, the specific source(s) of these lines must remain unspecified; close examination of the spectra of the mixtures composed of AdM_3 II, $FlexM_3$, and RCA (3 equiv) (Figures 9G and H) revealed a small line that appears to correspond to the higher field of these two unassigned lines.

Discussion

The purpose of this study was to determine if molecular simulations were capable of rationalizing the relative stabilities of 1 + 3 aggregates based on the CA·M rosette in solution in chloroform. In an effort to realize this goal, we developed a model of these systems based on Langevin dynamics. The

extent of the distortion of the $CA_3{\cdot}M_3$ rosette from planarity in a number of simulated aggregates correlated with the relative stabilities of the complexes determined experimentally. During the simulations, $HubM_3{\cdot}(RCA)_3$ forms the $CA_3{\cdot}M_3$ rosette with the lowest observed value of DP because it is geometrically compatible with a coplanar rosette and because its spokes are rigid; AdM_3 II$\cdot(RCA)_3$ has a propensity to place its $CA_3{\cdot}M_3$ rosette in a noncoplanar geometry, but is sufficiently rigid that its DP is lower than that of $FlexM_3{\cdot}(RCA)_3$; $FlexM_3{\cdot}(RCA)_3$ permits greater deviations from planarity because its spokes are more flexible. The potential advantage provided by the rigidity in the spokes of both AdM_3 I and II is nullified by their propensity to place their $CA_3{\cdot}M_3$ rosettes in noncoplanar geometries. This geometric constraint was the source of the larger values of DP, relative to $HubM_3{\cdot}(RCA)_3$, calculated for both AdM_3 I and II in the minimized structures and the Langevin models.

These calculations suggested that the criteria for formation of a stable complex are as follows: (i) an ability to form a planar $CA_3{\cdot}M_3$ rosette that allows for maximum hydrogen-bonding between groups and (ii) minimization of the conformational flexibility in the spokes of the tris-melamine to the level required to maintain a $CA_3{\cdot}M_3$ rosette with a low value of DP. These two preceding criteria for the formation of stable aggregates are an extension of the principle that preorganization is central to the binding capabilities of supramolecular complexes.[38,39]

The computations indicated that molecules of solvent in and around the complexes influence their stabilities. Clearly, the molecule of chloroform in the center of the complexes must be thought of as an integral part of the complex. The inference that it may be important for chloroform to occupy the center of the complexes should be taken into account when designing these structures, although this inference receives only partial support from the available experimental work.[40] Recent work by Still[41] has suggested a strong correlation between the stabilities of a host–guest system with the ability of the solvent to fit into a binding site of the host–guest aggregate. The role of solvent in our case was similar in spirit to these results in that the *size* of a molecule of solvent would be related to the stability of the aggregate. The behavior of other solvents that are too large to fit in the center are currently being explored experimentally and through computations.

The idea that triply hydrogen-bonded systems are more stable when coplanar has extensive precedent:[42-44] Using *deviations* from planarity as a measure of the relative stabilities of aggregates of the type presented here is a useful outcome of molecular modeling. CPK models of prospective complexes provided only basic qualitative information about the relative stabilities of aggregates; the information from MD calculations was (for the small number of aggregates examined) more reliable. For example, CPK models suggested that AdM_3 I$\cdot(RCA)_3$ would be stable; MD calculations, in agreement with experiment, indicated instability. MD calculations were also highly informative in suggesting a key role for solvent and suggesting that a single molecule of chloroform may be included in the central cavity of the $HubM_3{\cdot}(RCA)_3$ aggregate. In fact, according to these simulations, it might be best to consider the composition of these aggregates to be $HubM_3{\cdot}(RCA)_3{\cdot}CHCl_3$; the extent to which this inference describes reality remains to be determined experimentally.[40]

Experimental Section

1,3,5-Tris(4-iodophenyl)adamantane (2). Bis(trifluoroacetoxy)-iodobenzene (6.39 g, 14.85 mmol) was added to a solution of I_2 (3.43 g, 13.5 mmol) and 1,3,5–triphenyladamantane[45] (**1**) (3.29 g, 9.02 mmol) in $CHCl_3$ (60 mL) and the mixture was stirred at ambient temperature for 3 h under Ar. The reaction mixture was diluted with $CHCl_3$ (250 mL) and washed with 0.1 N $Na_2S_2O_3$ (4 × 50 mL). The colorless organic layer was washed with H_2O (50 mL) and brine (50 mL), dried over $MgSO_4$, filtered, and concentrated in vacuo to give **2** (6.29 g, 8.48 mmol, 94%): mp 255–7 °C; ^{1}H NMR (400 MHz, $CDCl_3$) δ 7.63 (d, 6 H, J = 8.49 Hz), 7.13 (d, 6 H, J = 8.55 Hz), 2.51 (m, 1 H), 1.98 (s, 6 H), 1.92 (d, 6 H, J = 2.69 Hz); ^{13}C NMR (100 MHz, $CDCl_3$) δ 149.20, 137.39, 127.12, 91.38, 47.59, 41.01, 38.14, 29.83; MS *m/z* 742 (M^+); HRMS calcd for $C_{28}H_{25}I_3$ (M^+) 741.9092, found 741.9100.

1,3,5-Tris(4-carboxyphenyl)adamantane (3). *tert*-Butyllithium (23.8 mL, 40.42 mmol, 1.7 M in pentane) was added to a solution of **2** (5.0 g, 6.74 mmol) in anhydrous THF (150 mL) at −78 °C under Ar. The mixture was stirred at −78 °C for 5 min. Carbon dioxide was bubbled through the mixture at −78 °C for 5 min, the cooling bath was removed, and CO_2 was bubbled through the mixture for an additional 45 min. The reaction mixture was diluted with H_2O (50 mL) and 1 N HCl (50 mL) and washed with EtOAc (3 × 50 mL). The combined organic layers were washed with brine (50 mL), dried over $MgSO_4$, filtered, and concentrated in vacuo. The residue was triturated with $CHCl_3$ (5 × 50 mL) to give **3** (2.64 g, 5.32 mmol, 79%): mp 223–5 °C (d); ^{1}H NMR (400 MHz, DMSO-d_6) δ 12.81 (bs, 3 H), 7.89 (d, 6 H, J = 8.24 Hz), 7.61 (d, 6 H, J = 8.33 Hz), 2.45 (bs, 1 H), 2.11 (d, 3 H, J = 11.94 Hz), 2.01 (d, 3 H, J = 12.05 Hz), 1.94 (s, 6 H); ^{13}C NMR (100 MHz, DMSO-d_6) δ 167.17, 154.73, 129.26, 128.26, 125.32, 46.53, 38.28, 29.45; MS *m/z* 495 ($M - H)^-$; HRMS calcd for $C_{31}H_{27}O_6$ ($M - H)^-$ 495.1808, found 495.1806.

AdM_3 I (5). Oxalyl chloride (79 μL, 909 mmol) was added to a solution of **3** (150 mg, 303 μmol) and DMF (30 μL) in anhydrous THF (3 mL), and the mixture was stirred at ambient temperature for 1 h under Ar. The reaction mixture was added to a flask charged with a solution of *o*-phenylenediamine melamine[3] **4** (274 mg, 909 μmol) and (i-Pr)$_2$NEt (475 μL, 2.73 mmol) in anhydrous THF (3 mL) at 0 °C under Ar. The resulting mixture was stirred at 0 °C for 20 min, the cooling bath was removed, and the mixture was stirred at ambient temperature for 12 h. The reaction mixture was concentrated in vacuo, and the residue was purified by SiO_2 chromatography (19:1 $CHCl_3$–CH_3OH) to give **5** (281 mg, 209 μmol, 69%): mp 108–10 °C (d); ^{1}H NMR (400 MHz, DMSO-d_6) δ 10.50, 10.37 (two conformers, bs, 3 H), 8.44, 8.34 (two conformers, bs, 3 H), 7.88 (d, 6 H, J = 8.10 Hz), 7.61–7.48 (bm, 12 H), 7.15 (bs, 6 H), 6.97, 6.78 (two conformers, bs, 3 H), 6.53, 6.41 (two conformers, bs, 6 H), 3.23–3.14 (m, 6 H), 2.48 (bs, 1 H), 2.15 (bs, 3 H), 2.06–1.95 (m, 9 H), 1.42–1.27 (m, 6 H), 0.82, 0.80 (two conformers, bs, 27 H); ^{13}C NMR (100 MHz, DMSO-d_6) δ 166.81, 166.44, 165.52, 164.34, 153.60, 132.87, 131.75, 130.63, 127.32, 125.87, 125.20, 124.69, 123.85, 123.47, 46.72, 42.90, 38.23, 36.37, 29.30, 29.23; MS *m/z* 1346 ($M + H)^+$; HRMS calcd for $C_{76}H_{92}N_{21}O_3$ ($M + H)^+$ 1346.7702, found 1346.7721; MS ion profile calcd for $C_{76}H_{92}N_{21}O_3$ ($M + H)^+$ *m/z* (relative intensity) 1346 (100), 1347 (93), 1348 (44), 1349 (13), found 1346 (100), 1347 (84), 1348 (39), 1349 (13).

AdM_3 II (7). Oxalyl chloride (57 μL, 652 μmol) was added to a solution of **3** (108 mg, 217 μmol) and DMF (100 μL) in anhydrous THF (3 mL) and the mixture was stirred at ambient temperature for 1 h under Ar. The reaction mixture was added to a flask charged with a solution of *m*-xylylene diamine melamine[46] **6** (310 mg, 652 μmol) and (i-Pr)$_2$NEt (350 μL, 2.0 mmol) in anhydrous THF (3 mL) at 0 °C under Ar. The resulting mixture was stirred at 0 °C for 1 h, the cooling bath was removed, and the mixture was stirred at ambient temperature

(38) Cram, D. J. *Angew. Chem., Int. Ed. Engl.* **1988**, *27*, 1009.
(39) Cram, D. J.; deGrandpre, M.; Knobler, C. B.; Trueblood, K. N. *J. Am. Chem. Soc.* **1984**, *106*, 3286.
(40) Simanek, E. E.; Whitesides, G. M. Unpublished results.
(41) Chapman, K. T.; Still, W. C. *J. Am. Chem. Soc.* **1989**, *111*, 3075.
(42) Pitsch, S.; Wendeborn, S.; Jaun, B.; Eschenmoser, A. *Helv. Chim. Acta* **1993**, *76*, 2161.
(43) Zerkowski, J. A.; Seto, C. T.; Whitesides, G. M. *J. Am. Chem. Soc.* **1992**, *114*, 5473.
(44) Zerkowski, J. A.; Seto, C. T.; Wierda, D. A.; Whitesides, G. M. *J. Am. Chem. Soc.* **1990**, *112*, 9025.
(45) Newman, H. *Synthesis* **1972**, 692.
(46) Mathais, J. P.; Seto, C. T.; Whitesides, G. M. *J. Am. Chem. Soc.* **1994**, *116*, 1725.

for 18 h. The reaction mixture was concentrated in vacuo, and the residue was purified by SiO_2 chromatography (33:1 $CHCl_3$–CH_3OH) to give **7** (203 mg, 109 μmol, 50%): mp 143–5 °C; ^1H NMR (400 MHz, DMSO-d_6) δ 7.49 (bs, 6 H), 7.35 (bs, 12 H), 7.27–6.94 (m, 18 H), 6.89 (bs, 3 H), 6.42, 6.32 (two conformers, bs, 3 H), 6.01, 5.93 (two conformers, bs, 6 H), 4.44 (bs, 12 H), 4.29 (bs, 6 H), 3.16 (bs, 6 H), 2.42 (m, 1 H), 2.06–1.90 (m, 12 H), 1.34 (bs, 6 H), 1.26, 1.23 (two conformers, two s, 27 H), 0.90–0.64 (bm, 27 H); ^{13}C NMR (100 MHz, DMSO-d_6) δ 170.98, 166.20, 165.98, 151.01, 149.57, 133.59, 126.47, 126.30, 125.30, 125.15, 42.84, 37.94, 35.42, 34.14, 31.08, 29.27; MS *m/z* 1870 ($M(^{13}C_2) + H)^+$; MS ion profile calcd for $C_{115}H_{146}N_{21}O_3$ $(M + H)^+$ *m/z* (relative intensity) 1869 (73), 1870 (100), 1871 (69), 1872 (32), 1873 (11), found 1869 (85), 1870 (100), 1871 (63), 1872 (29), 1873 (10).

Acknowledgment. This research was supported by the National Science Foundation Grant (CHE-91-223331). D.M.G. was the recipient of a NIH postdoctoral fellowship (1F32 CA09326-01). We would like to thank Molecular Simulations Inc., and the University of Massachusetts Lowell for generous donations of computer time.

Supplementary Material Available: A summary of the parameters used and ACFs for the torsional families 1–3, 5, and 8 (10 pages). This material is contained in many libraries on microfiche, immediately follows this article in the microfilm version of the journal, and can be ordered from the ACS; see any current masthead page for ordering information.